Electrochimica Acta 555 (2026) 148414

Contents lists available at ScienceDirect

Electrochimica Acta

journal homepage: www.journals.elsevier.com/electrochimica-acta

Chitosan as a corrosion inhibitor for gray cast iron and its role in mitigating the stiction phenomenon in automotive braking systems

Michele Motta [a,*], Agusti Sin [b,c], Alfredo Rondinella [a], Lorenzo Fedrizzi [a], Francesco Andreatta [a]

[a] University of Udine, Polytechnic department of engineering and architecture, Via del Cotonificio 108, 33100 Udine, Italy
[b] ITT- Friction Technologies, Via Molini 19, 12032 Barge CN, Italy
[c] Joint Lab ITT- UniTO, via Quarello 15, 101135 Torino (TO), Italy

ARTICLE INFO

Keywords:
Gray cast iron
Corrosion inhibitor
Chitosan
Stiction phenomenon

ABSTRACT

The corrosion inhibition effect of high molecular weight chitosan on gray cast iron discs for automotive applications was investigated using potentiodynamic polarization (PDP) and electrochemical impedance spectroscopy (EIS) in a 0.1 M HCl solution containing 0.8, 1.5, and 3 gl^{-1} of the inhibitor. The results suggest that, after 1 h of immersion in the chitosan-containing solutions, gray cast iron shows a modest reduction in cathodic current density, whereas no significant changes are observed in the anodic behavior. Scanning Kelvin probe force microscopy (SKPFM) confirmed the formation of an adsorbed inhibitor film over the cathodic sites at this early stage. To evaluate the stability of the polymer, PDP measurements were conducted after 48 h of immersion, revealing a significant reduction in corrosion rate and notable inhibition efficiency across all tested concentrations. EIS analysis corroborated these findings, indicating the formation of an adsorbed layer of chitosan covering the entire surface of the gray cast iron samples. The protective effect of this layer was primarily attributed to the blanketing of active sites on the metal surface. Finally, the presence and integrity of the inhibitor films were confirmed through scanning electron microscopy (SEM) and attenuated total reflectance – Fourier transform infrared spectroscopy (ATR-FTIR).

1. Introduction

In commercial vehicles, rotors are frequently manufactured from gray cast iron. This material is a rather complex material from a metallurgical view point, with a particularly heterogenous structure composed of “A type” graphite flakes in a pearlitic matrix often containing ferrite. This material is widely chosen due to its cost-effectiveness, favorable wear resistance, high thermal conductivity, and inherent vibration-damping properties [1,2]. Despite these advantages, the electrochemical heterogeneity between the graphite inclusions and the surrounding pearlitic matrix promotes localized galvanic corrosion in the presence of an electrolyte. As a result, corrosion of the gray cast iron disc may lead to several issues connected to the safety and the reliability of the braking system. Furthermore, brake disc corrosion contributes to the release of pollutants, presenting additional environmental challenges [3]. Addressing these issues is critical for the development of sustainable and environmentally friendly braking systems in the context of modern vehicles, especially for electric vehicles (EVs). In this frame, the integration of regenerative braking systems has significantly reduced reliance on traditional hydraulic braking systems, particularly in urban driving conditions, where regenerative braking accounts for approximately 90 % of braking activity. This shift in braking system design drives the development of advanced friction materials that not only minimize particulate emissions but also exhibit enhanced wear resistance and effectively address corrosion-related issues [4]. The accumulation of corrosion products on the surface of the gray cast iron disc during prolonged periods of inactivity and the limited use of the traditional braking system in electric vehicles can lead to the stick-slip phenomenon and to stiction, which consist of the strong adhesion of friction material to the disc surface, potentially compromising the reliability and performance of the braking system[1,4–6].

To mitigate corrosion related issues, metallic zinc is commonly employed as an additive in current friction material formulations. However, regulatory measures, such as the European Union’s Euro 7 standards, are intensifying efforts to reduce brake particle emissions and limit the use of heavy metals in friction material compositions [7–10].

* Corresponding author.
E-mail address: michele.motta@uniud.it (M. Motta).

https://doi.org/10.1016/j.electacta.2026.148414
Received 14 January 2026; Received in revised form 6 February 2026; Accepted 7 February 2026
Available online 9 February 2026

Consequently, there is a growing need to identify and develop new, more environmentally friendly corrosion inhibitors that can replace metallic zinc in automotive friction materials. The integration of regenerative and traditional braking systems in EV's reduces brake pad temperature during braking, opening the possibility to investigate more thermally sensitive organic corrosion inhibitors for the first time [2,5]. When selecting an organic corrosion inhibitor suitable for incorporation into friction materials, it is essential to achieve an appropriate balance among inhibition efficiency, economic viability, and, most critically, toxicity. In the present study, chitosan was identified as a feasible candidate capable of meeting these requirements.

Chitosan is a well-known natural heteropolysaccharide with a chain structure composed of a random distribution of D-glucosamine and N-acetyl-D-glucosamine connected together by 1.4 glycosidic linkage [11]. Its annual production is estimated to be equal to one billion tons per year, and the main source is the chitin extracted from the shells of crustacean sea food [12]. Chitosan is a biocompatible, biodegradable, and non-toxic polymer that is widely employed in the medical and food fields [13,14]. From a corrosion perspective, the presence in the structure of chitosan of different polar groups, capable of establishing an interaction with the metal surface, makes chitosan an interesting compound as a green corrosion inhibitor [15].

Up to date, the application of pure chitosan as a green corrosion inhibitor has not been frequently reported in the literature especially due to its low solubility in aqueous solutions [16,17], while it has been mainly studied in acidic conditions [12,15,16,18]. Chitosan is basically insoluble in organic solvents and water at a pH higher than 6.5, while it is soluble only in slightly acidic solutions. This is due to the protonation of the glucosamine-NH_2 and the hydroxyl (-OH, -CH_2OH) units into the more soluble cationic forms [11]. Chitosan can be solubilized when a degree of protonation higher than 50 % is reached [18]. Furthermore, the solubility in aqueous solutions of chitosan exhibits a positive correlation with the degree of deacetylation, while it decreases with an increase in molecular weight [18,19]. Similarly, a temperature increase has been reported to have a detrimental effect on the solubility of medium molecular weight chitosan in acetic acid solution [18]. Chitosan for industrial applications has a deacetylation degree ranging between 60 and 100 % and an average molecular weight of 3800–20,000 Da [11].

Three main strategies have been explored to improve the solubility and corrosion-inhibition performance of chitosan. A first approach involves the use of chitosan oligosaccharides, low-molecular-weight degradation products of chitosan that retain free amino groups and complete water solubility [20]. N-propyl chitosan oligosaccharide quaternary ammonium salt (PHC) and N-benzyl chitosan oligosaccharide quaternary ammonium salt (BHC) were synthetized and characterized as corrosion inhibitors for P110 steel in a 3.5 % NaCl CO_2 saturated solution. With both inhibitors, the formation of a protective film reduced the surface roughness, presenting a corrosion inhibition efficiency higher than 90 %, which was observed in electrochemical impedance measurements for both inhibitors after 1 h of immersion of the steel sample in the electrolyte solution with 100 mgl^{-1} of inhibitors [17].

A second strategy is the chemical modification of the polymer backbone, taking advantage of chitosan's amino and hydroxyl groups to graft functional moieties. Polyethylene glycol (PEG) functionalization has been widely investigated, producing crosslinked chitosan-PEG polymers with improved solubility and inhibition efficiencies around 90 % for mild steel in 1 M HCl electrolyte solution [18,21,22].

A third approach involves grafting corrosion-active heterocycles or chelating groups onto chitosan. Triazole-, 8-hydroxyquinoline-, and other organic moiety-modified chitosans have demonstrated high solubility in acidic media and inhibition efficiencies exceeding 90–95 %, attributed to strong chemical adsorption [23–30]. The presence of a protective film can also be justified in terms of the complexation between the inhibitors and the metal [11]. Indeed, chitosan and its derivatives are known to promote the complexation of several metallic ions and to form films in combination with inorganic and metallic particles [31–35].

Despite chemically modified forms of chitosan being extensively discussed in literature, only a few studies discuss the effect of pure chitosan as an organic corrosion inhibitor [12,36–39]. Nevertheless, the restricted solubility of chitosan in acidic conditions may be an advantage for the application of chitosan as an anti-corrosive additive placed directly into the friction material.

In the typical disc–friction material assembly, acidic conditions can develop within the occluded zones at the interface between the disc and the friction layer for instance when the parking brake is activated and conditions favorable to crevice corrosion are established at this interface. Incorporating chitosan directly into the friction material offers two main advantages. First, its limited solubility may mitigate leaching under wet conditions. Second, chitosan can be released from the bulk in a controlled manner, triggered specifically by the localized decrease in pH at the disc–friction material interface.

In the present work we decided to focus on the effect of chitosan on the corrosion of the gray cast iron disc in an acidic solution simulating the occluded cell condition. The corrosion behavior of gray cast iron, both in the absence and presence of the inhibitor, was investigated using potentiodynamic polarization (PDP) and electrochemical impedance spectroscopy (EIS) measurements. Scanning Kelvin probe atomic force microscopy was further used to gain information regarding the inhibition mechanism that was further investigated using FE-SEM and ATR-FTIR.

2. Experimental procedure

2.1. Materials

Gray cast iron brake discs with the average composition based on XRF analysis, reported in Table 1, were provided by ITT.

High molecular weight chitosan was purchased from Sigma-Aldrich and directly used without further modification. Hydrochloric acid (HCl) 37 % was purchased by VWR International and appropriately diluted to obtain a 0.1 M HCl solution that was used as an electrolyte solution for the electrochemical characterization. An acidic electrolyte solution was employed to account for the acidification arising from the formation of an occluded cell at the rotor–pad interface under effective static contact conditions between the rotor and the brake pad. Electrochemical measurements were performed to investigate the influence of this acidification on the corrosion behavior of the gray cast iron disc associated with this contact condition, which are typical of stiction phenomena in automotive braking systems. Owing to the strongly acidic nature of the solution, which simulates the acidification caused by oxygen depletion at the disc–pad interface under real service conditions, the electrolyte was not deaerated, as the cathodic reaction was predominantly governed by proton reduction.

2.2. Electrochemical measurements

Potentiodynamic polarization and electrochemical impedance spectroscopy were employed to evalutae possible direct absorption of high molecular weight chitosan or formation of complexes with corrosion products on the surface of the gray cast iron disc. For electrochemical tests, samples with 2 cm diameter were cored from the gray cast iron discs. Electrochemical measurements were conducted using a three-electrode setup. The gray cast iron samples were used as working electrodes (WE), a graphite bar was the counter electrode (CE), and a 3 M KCl Ag/AgCl electrode was employed as reference electrode (RE). All measurements were carried out using an electrochemical cell designed to expose a 1 cm^2 area of the working electrode to the electrolyte. A PTFE gasket ensured proper sealing, and a copper strip was used to electrically connect the non-exposed surface of the working electrode to the electrochemical workstation.

The WE area was 1 cm^2. The WE samples were prepared with silicon

Table 1
Chemical composition in weight percentage ($\%_w$) of the gray cast iron disc provided by ITT.

Element	Fe	C	Si	Cu	Mn	Cr	S	P	Other elements	TOT
$\%_w$	94.4	2.7	1.6	0.12	0.8	0.07	0.06	0.04	0.21	100

carbide grinding paper up to grit 2000, cleaned in ethanol, rinsed with deionized water, and stored in a sealed environment in the presence of silica gel for 48 h before every measurement. The inhibitor efficiency was assessed by employing three different concentrations of high molecular weight chitosan in the 0.1 M HCl solution, 0.8, 1.8, and 3 gl^{-1}. In order to secure a stable potential before every polarization, all the measurements were conducted after 1 h of exposure to the electrolyte solution. The measurements were also repeated after 48 h of exposure. The polarization curves were recorded by performing independent scans in the cathodic and anodic directions with a scan rate of 0.2 mVs^{-1}. Cathodic scans were initiated at −500 mV vs. RE and extended to −1000 mV vs. RE, whereas anodic scans were performed from an initial potential of −600 mV vs. RE up to 500 mV vs. RE. A minimum of three different repetitions were acquired for each scan. For the measurements conducted after 48 h of immersion, the inhibition efficiency was calculated according to:

$$\eta = (1 - I_{inh}/I_0) * 100 \quad (1)$$

where I_{inh} is the corrosion current density in the presence of high molecular weight chitosan in the electrolyte solution, and I_0 is the current density in the electrolyte without inhibitor.

Electrochemical impedance spectroscopy was performed by means of an Autolab PGSTAT 30 potentiostat at OCP in the frequency range from 10 KHz to 0.01 Hz (8 points per decade), applying a sinusoidal perturbation of 10 mV amplitude. Spectra were collected using 0.1 M HCl solution with 0.8, 1.8, and 3 gl^{-1} of high molecular weight chitosan for immersion times up to 9 days. The inhibition efficiency was calculated from EIS data according to the following equation:

$$\eta = (1 - Rp_0/Rp_{inh}) * 100 \quad (2)$$

where Rp_0 is the polarization resistance in the electrolyte without the inhibitor and Rp_{inh} represent the polarization resistance in the electrolyte containing the inhibitor.

2.3. Scanning Kelvinprobe force microscopy

A Nanoscope III Multimode AFM equipped with an Extender TM Electronic Module for Volta potential measurement (SKPFM) was employed to evaluate the effect of high molecular weight chitosan on the surface potential of the gray cast iron. The AFM was operated in tapping mode to record the surface topography, during which the vertical deflection of the cantilever was monitored using a laser focused on extremity of the cantilever. In parallel, the Kelvin probe module was used in lift mode to map the Volta potential distribution across the surface. All SKPFM measurements were conducted using an aspect ratio of 1, with areas of 50 × 50 and 30 × 30 μm. The topographic and surface potential maps were acquired using *n*+-silicon tips with a $PtIr_5$ coating. The scan frequency was 0.2 Hz and the scan height in lift mode was 100 nm. Measurements were first performed on mirror-polished gray cast iron samples and then repeated on the same areas after 1 h of immersion in a 0.1 M HCl solution containing 3 gl^{-1} of high molecular weight chitosan.

2.4. FE-SEM and IR characterization

FE-SEM (FE-SEM Jeol USA JSM-7600F) with a 15 kV accelerating voltage and a Nicolet iS 50 FT-IR instrument (Thermofisher Waltham, Massachusetts, USA) in attenuated total reflectance mode (ATR) were further used in order to gain information regarding the inhibition mechanism. Each IR spectrum was acquired using a resolution of 2 cm^{-1} in a spectral window ranging from 500 to 4000 cm^{-1}, with 32 scans.

3. Results and discussion

3.1. Potentiodynamic polarizationand SKPFM

Fig. 1 shows the potentiodynamic polarization curves after 1 h of immersion obtained by varying the concentration of in the HCl 0.1 M solution containing different amounts of high molecular weight chitosan.

After one hour of exposure to the electrolyte solution, it can be stated that high molecular weight chitosan exhibits only a limited effect toward the corrosion of the gray cast iron specimen. Moreover, the presence of chitosan does not produce a substantial alteration in the overall pattern of the potentiodynamic curves, indicating that the inhibition mechanism is mainly linked to the blanketing of the surface rather than a change in the electrochemical reaction mechanisms. Based on the observed shift in corrosion potential, high molecular weight chitosan may be categorized as a mixed-type inhibitor. Nonetheless, the cathodic curves in Fig. 1A seems to indicate a slightly preferential adsorption of the inhibitor on the cathodic regions of the surface (graphitic flakes).

The SKPFM was used to study the preferential adsorption of chitosan on the cathodic sites of the surface for a short immersion time. A mirror-polished gray cast iron sample was initially characterized using the field-emission microscope to highlight the presence of a suitable spot on the surface of the sample for the AFM characterization (Fig. 2A). The same area visible in the FE-SEM area was successively analyzed using the SKPFM. The FE-SEM image and the Volta potential map of this area are shown in Fig. 2A and B, respectively. The Volta potential map (Fig. 2B) displays a marked potential contrast between the graphite flake and the gray cast iron matrix, with the flake displaying a more positive potential relative to the matrix. This potential difference is about 300 mV, indicating a strong galvanic coupling between the graphite flake and the matrix. The same sample was successively immersed in the 0.1 M HCl electrolyte solution containing 3gl^{-1} of high molecular weight chitosan. After 1 h of immersion, the sample was recovered, washed with distilled water, and carefully dried in order to repeat the analysis of the Volta potential. Fig. 2C shows a magnification of the Volta potential measured in the same region, over the cathodic flake of Fig. 2B after 1 h of immersion in the electrolyte solution in the presence of high molecular weight chitosan. By comparing Fig. 2B and Fig. 2C, it can be seen that the Volta potential contrast between the graphite flake and the matrix is strongly reduced. This is most likely related to the adsorption of high molecular weight chitosan on the graphitic flake. Indeed, the preferential absorption of chitosan toward the cathodic sites of the surface of ferrous material was also reported by Gupta et al. [12] and Solomon et al. [36], respectively studying the corrosion of mild steel in sulfamic acid solution and sulfuric acid solution. Thus, in line with the potentiodynamic polarization measurements presented in Fig. 1A, the preferential adsorption of high molecular weight chitosan on the cathodic sites of the sample during the first hour of immersion can be confirmed for the gray cast iron sample.

The stability and efficiency of high molecular weight chitosan with the time of immersion were then further studied by repeating the measurements for an immersion time of 48 h.

Fig. 3 shows the most representative potentiodynamic polarization curves obtained in the presence of high molecular weight chitosan at various concentrations after 48 h of immersion in the acidic solution. Table 2 reports the corrosion potentials, corrosion current densities, and inhibition efficiencies obtained by applying the Tafel extrapolation.

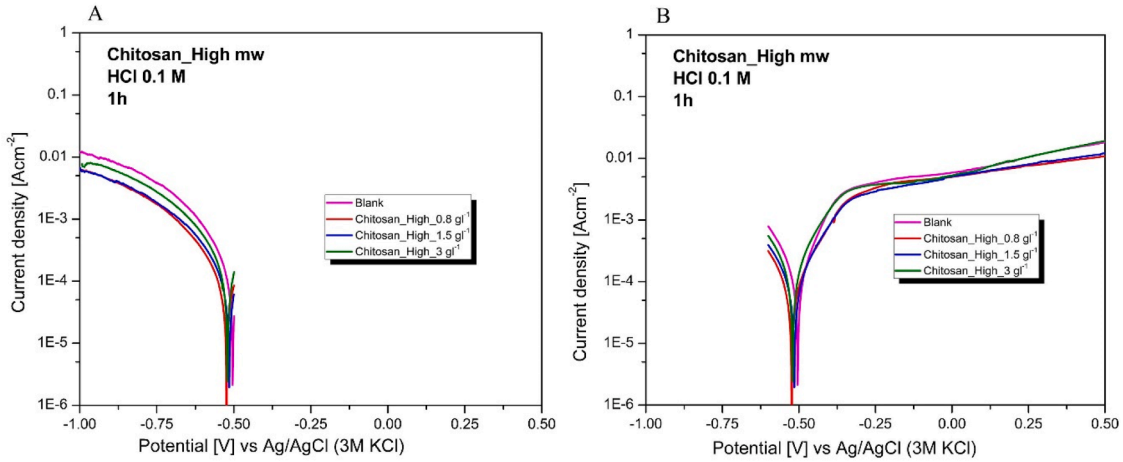

Fig. 1. Cathodic potentiodynamic polarization curves obtained after 1 h of immersion in a HCl 0.1 M solution without inhibitor and with 0.8, 1.5, and 3 gl^{-1} of high molecular weight chitosan (A), Anodic potentiodynamic polarization curves obtained after 1 h of immersion in a HCl 0.1 M solution without inhibitor and with 0.8, 1.5, and 3 gl^{-1} of high molecular weight chitosan (B).

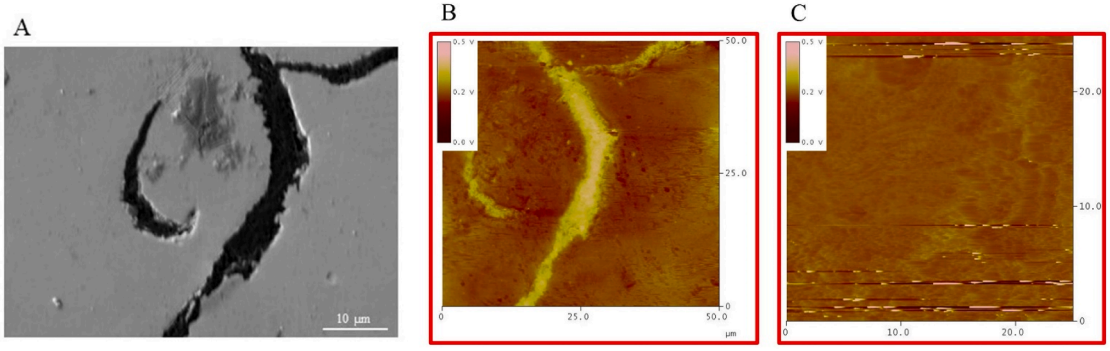

Fig. 2. FE-SEM image of a graphitic flake on the surface of a mirror-polished gray cast iron sample (A), SKPFM analysis of the graphitic flakes presented in A (B), Surface potential map of the same region after 1 h of immersion in a 0.1 M HCl electrolyte solution containing 3gl^{-1} of high molecular weight chitosan (C).

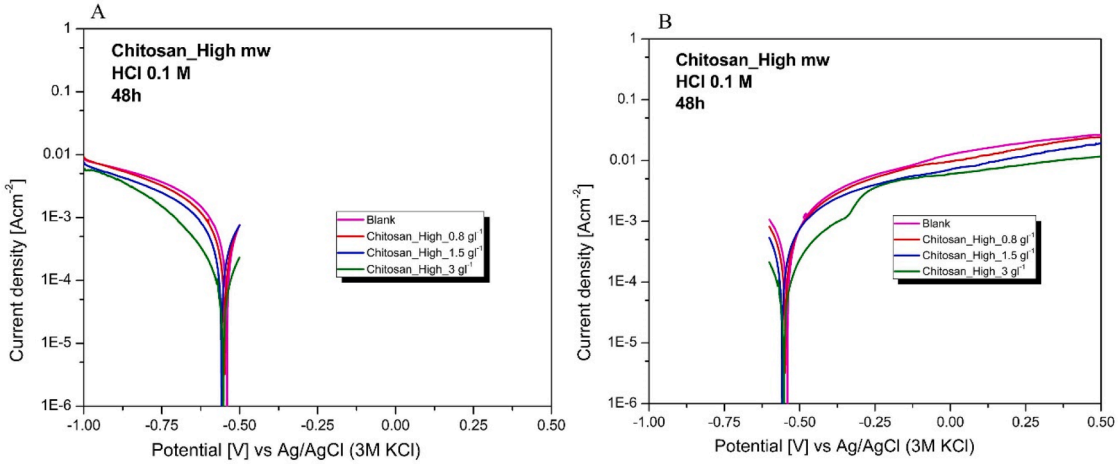

Fig. 3. Cathodic potentiodynamic polarization curves obtained after 48 h of immersion in a HCl 0.1 M solution without inhibitor and with 0.8, 1.5, and 3 gl^{-1} of high molecular weight chitosan (A), Anodic potentiodynamic polarization curves obtained after 48 h of immersion in a HCl 0.1 M solution without inhibitor and with 0.8, 1.5, and 3 gl^{-1} of high molecular weight chitosan (B).

In agreement with the findings of Okoronkwo et al. [37] and Rabizadeh and Asl [38], the corrosion inhibition performance of high molecular weight chitosan on gray cast iron was observed to improve for prolonged immersion times and increasing the inhibitor concentration. As the concentration was raised from 0.8 to 3 gl^{-1}, a marked decrease in current density was observed in both the cathodic (Fig. 3A) and anodic (Fig. 3B) branches of the curves. The Tafel extrapolation analysis revealed a corrosion current density reduction of 35 % at 0.8 gl^{-1}, 51 % at 1.5 gl^{-1}, and approximately 79 % at the highest concentration of 3 gl^{-1} (Table 2).

Table 2
Corrosion potentials (Ecorr), corrosion current densities (Icorr), and inhibition efficiencies values (η) obtained from the potentiodynamic polarization measurements after 48 h of immersion in a HCl 0.1 M electrolyte solution without inhibitor and with 0.8, 1.5, and 3 gl^{-1} of high molecular weight chitosan. The σ values are the standard deviations of each parameter for the three experiments conducted for each analysis.

Inhibitor	Concentration [gl^{-1}]	E_{corr} [mV]	σ_E_{corr} [mV]	I_{corr} [$mAcm^{-2}$]	σ_E_{corr} [$mAcm^{-2}$]	η [%]	σ_η [%]
Blank	-	−542	0.7	1.08	0.01	-	-
Chitosan High mw	0.8	−552	9	0.70	0.20	35	18
	1.5	−549	16	0.52	0.30	51	28
	3	−543	10	0.22	0.07	79	7

The enhanced performance of high molecular weight chitosan at higher concentrations for longer times of immersion can be ascribed to a more extensive and uniform surface coverage, arising from improved adsorption of the inhibitor molecules onto the sample surface. The relatively high standard deviations reported in Table 2 for the lower concentrations (0.8 and 1.5 gl^{-1}) may be associated with partial degradation of the polymer during prolonged immersion in the aggressive environment. Nevertheless, the higher inhibition efficiency observed at elevated concentrations, coupled with the relatively low standard deviation (Table 2), indicates that the adsorbed chitosan layer formed with higher concentrations of the polymer gives rise to a more stable and adherent protective film on the surface of the sample. Indeed, the polarization curve in Fig. 2 shows a marked reduction of both the cathodic and anodic current density in the presence of 3 gl^{-1} of high molecular weight chitosan in the acidic electrolyte. In this case, chitosan acts as a mixed corrosion inhibitor, and, besides the strong adsorption on the cathodic sites, the pseudo-passive range in the anodic branch of the curve suggests the stabilization of the inhibitor layer, in which the plausible formation of complexes between the inhibitor and corrosion products cannot be excluded.

3.2. *Electrochemical impedance spectroscopy*

In order to further assess the filming ability of high molecular weight chitosan, EIS was used to study the behavior of the gray cast iron up to 9 days of immersion in the 0.1 M HCl solution. To this end, open-circuit potential (OCP) measurements were conducted to assess the stability of the system under study.

Fig. 4A presents the OCP measurements for the main representative samples prior to the polarization analyses reported in Fig. 3. The data indicate that the presence of chitosan in the electrolyte enhances system stability, whereas the OCP fluctuations observed for the blank sample may be attributed to the formation of a soluble, non-protective layer of corrosion products. Fig. 4B shows a magnification of the OCP measurements during the initial hours of immersion. After 1 h, all samples, including the blank, exhibited potential variations of only a few μV. Therefore, the impedance analysis was initially performed after an immersion time of 1 h.

Fig. 5 presents the Nyquist (Fig. 5A) and Bode plots (Fig. 5B) for the blank solution after 1 h, 2 days, and 9 days of immersion in the acidic electrolyte. The results clearly demonstrate that, in 0.1 M HCl, gray cast iron exhibits limited corrosion resistance, as reflected by the relative low impedance module at low frequencies (Fig. 5B).

After approximately 2 days of immersion, and subsequently for longer immersion periods, a second time constant becomes evident in the Nyquist and the Bode plots (Fig. 5). This feature is most likely associated with the gradual development of a layer of corrosion products on the cast iron surface. However, this layer appears to be non-protective and susceptible to mechanical degradation. As a result, the cast iron surface fails to attain a stable electrochemical condition and exhibits pronounced uniform corrosion and a continuous reduction of the impedance module with the time of immersion.

Fig. 6 reports Nyquist and Bode plots of the impedance for high molecular weight chitosan after 1 h, 2 days, and 9 days of immersion. Data reported in Fig. 6 display an overall increase of the impedance due to the presence of the inhibitor.

To obtain information regarding the electrochemical behaviour of the samples, the impedance data, including the one reported in Fig. 5, were fitted using Zview and the equivalent circuits reported in Fig. 7. In particular, the Randles equivalent circuit was used to fit the impedance data after 1 h of immersion, while a two-time constants circuit was used to fit the data for longer times of immersion. The presence of a second time constant in the Nyquist and Bode plots for longer times of immersion (Fig. 6) indicates the formation of a secondary layer of adsorbed inhibitor and corrosion products on the surface in line with polarization curves and Volta potential maps discussed above.

In Fig. 7, R1 represents the charge-transfer resistance associated with the electrochemical processes occurring at the active gray cast iron surface, whereas R2 is used to model the resistance of the surface film composed of adsorbed inhibitor and corrosion products. The overall

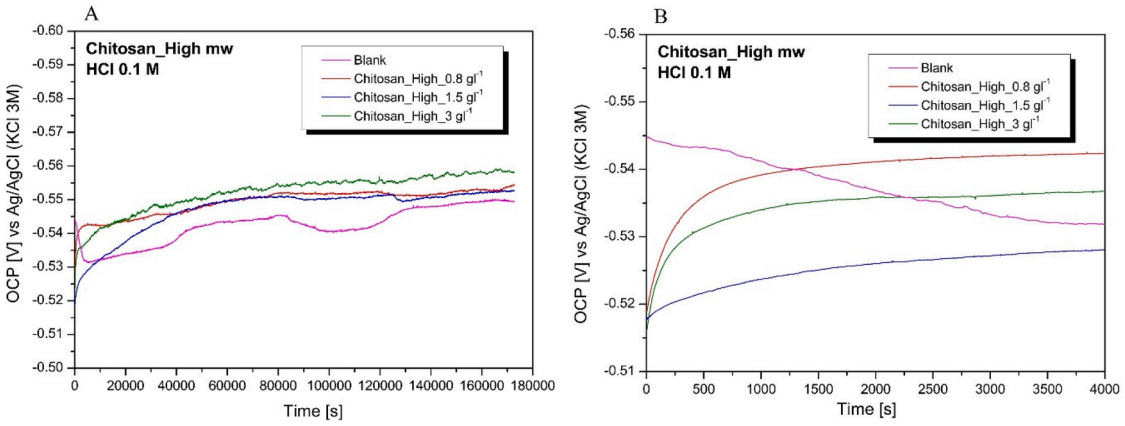

Fig. 4. Open-circuit potential (OCP) measurements over 48 h of immersion in the various electrolyte solutions studied (A), magnified view of the initial hours of immersion (B).

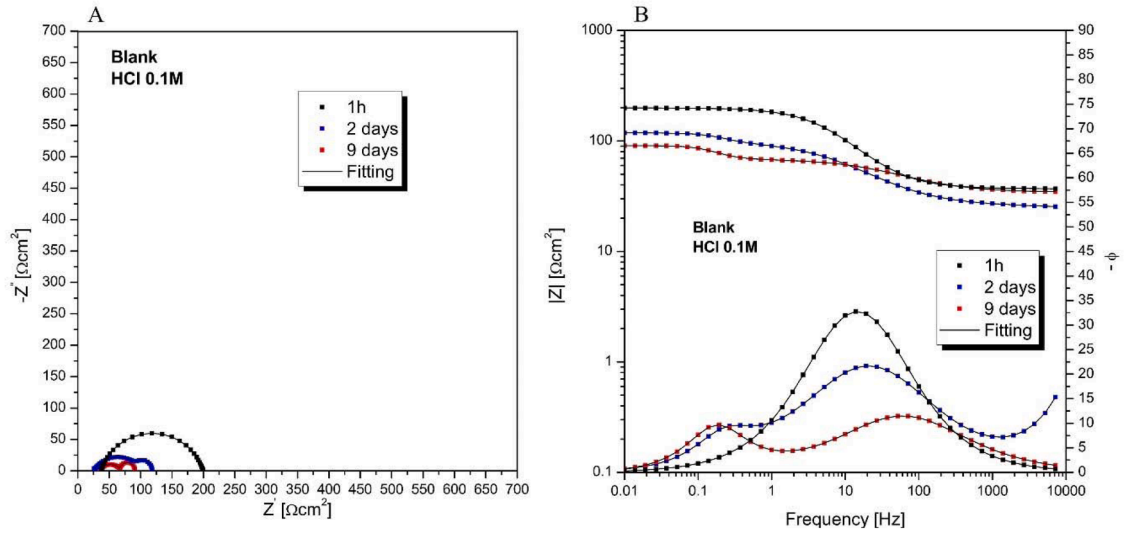

Fig. 5. Nyquist plots up to 9 days of immersion of the gray cast iron disc in the HCl 0.1 M solution (A), Bode plots up to 9 days of immersion of the gray cast iron disc in the HCl 0.1 M solution (B).

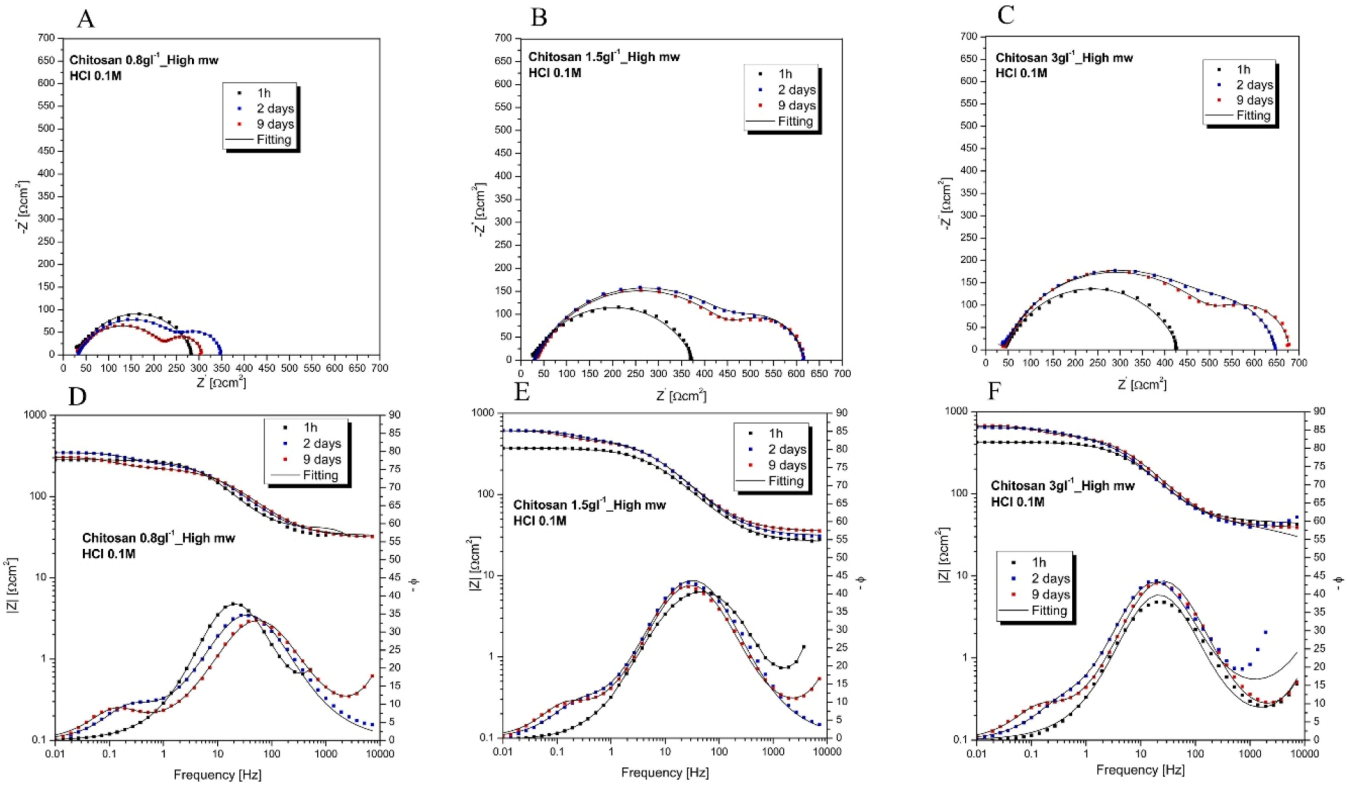

Fig. 6. Nyquist and Bode plots up to 9 days of immersion of the gray cast iron disc in the HCl 0.1 M solution containing high molecular weight chitosan with concentration of 0.8 gl^{-1} (A-D), 1.5 gl^{-1} (B-E), and 3 gl^{-1} (C-F).

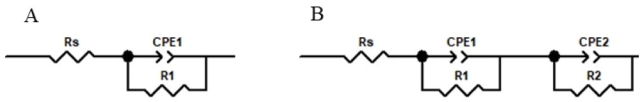

Fig. 7. Equivalent circuit used to fit the data reported in Fig. 5 and Fig. 6 after 1 h of immersion (A), Equivalent circuit used to fit the data for longer immersion times (B).

polarization resistance, Rp (Rp = R1 + R2), was used as an indication of the corrosion resistance of the system. The values of R1, R2, and Rp obtained from fitting the experimental data reported in Fig. 5 and Fig. 6 are summarized in Table 3.

The initial adsorption of high molecular weight chitosan onto the cathodic sites of the gray cast iron surface contributes to the observed increase of polarization resistance (Rp) as indicated by the cathodic polarization measurements obtained after 1 h of immersion (Fig. 1) and by the results presented in Table 3 and Fig. 6, This effect is evident for all the concentrations examined and leads to higher resistance values relative to the blank sample after 1 h of immersion in the electrolyte

Table 3
Results obtained from the fitting of the data reported in Fig. 5 and Fig. 6 using the equivalent circuits presented in Fig. 7.

Concentration [gl^{-1}]	Time	R_1 [Ωcm^2]	R_2 [Ωcm^2]	R_p [Ωcm^2]	Y_1^0 [$\mu\Omega^{-1}s^n cm^{-2}$]	Y_2^0 [$\mu\Omega^{-1}s^n cm^{-2}$]	n_1	n_2	η	σ_η [%]
-	1 h	163	-	163	369	-	0.8	-	-	-
	2 days	74	20	94	1000	38,300	0.7	1	-	-
	9 days	35	21	56	782	47,200	0.7	1	-	-
0.8	1 h	270	-	270	298	-	0.7	-	40	14
	2 days	236	80	316	229	10,900	0.7	1	71	15
	9 days	209	71	280	198	21,215	0.7	1	80	12
1.5	1 h	354	-	354	193	-	0.7	-	54	2
	2 days	469	114	583	170	7918	0.7	1	84	3
	9 days	457	126	583	179	12,000	0.7	1	90	1
3	1 h	396	-	396	197	-	0.7	-	59	18
	2 days	564	52	616	231	18,849	0.7	1	85	7
	9 days	504	138	642	163	11,078	0.8	1	91	9

solution. Furthermore, while the blank sample displays a progressive decrease of the polarization resistance (Rp) with the time of immersion, in agreement with the polarization analysis reported in Fig. 3, there is an evident increase of the polarization resistance after 2 days of immersion for the solution containing high molecular weight chitosan for all the concentrations studied.

It is important to note that, in the presence of high molecular weight chitosan, the major contribution to the overall polarization resistance appears to be associated with the charge-transfer resistance R1, rather than with the film resistance R2. In fact, whereas the charge-transfer resistance of the blank sample consistently decreases with increasing immersion time, this trend is not observed when higher concentrations of high molecular weight chitosan are present in the electrolyte solution. Notably, although a slight decrease of charge-transfer resistance is observed for the 0.8 gl^{-1} high molecular weight chitosan solution after 2 days of immersion, a pronounced increase in R1 is recorded for the 1.5 and 3 gl^{-1} solutions. Only after 9 days of immersion, it was possible to observe a reduction of the charge-transfer resistance for all the concentrations investigated. Nevertheless, while the blank sample exhibited a charge-transfer resistance of 35 $\Omega \cdot cm^2$, the presence of 0.8, 1.5, and 3 gl^{-1} high molecular weight chitosan still resulted in considerably higher values of 209, 457, and 504 $\Omega \cdot cm^2$, respectively. After 9 days of immersion in the presence of chitosan, slightly higher values of the film resistance R2 can also be observed. However, these increases are modest relative to the blank sample, and therefore no definitive conclusions can be drawn based solely on the behavior of the film resistance.

Based on these results, the protection mechanism of high molecular weight chitosan seems not related to the formation of an adsorbed film with insulating properties; rather, the adsorption of chitosan may act by blanketing the surface, reducing the active area of the gray cast iron disc in contact with the corrosive electrolyte.

The polarization resistance values obtained from the fitting procedure were subsequently used to calculate the inhibition efficiency according to Eq. (2) (Table 3). When compared with the efficiencies derived from polarization measurements (Table 2), a similar trend is observed. However, the values obtained via EIS are consistently higher than those obtained from PDP. This discrepancy can be reasonably attributed to the different electrochemical properties provided by the two techniques. While polarization measurements involve a substantial perturbation of the system, EIS represents a low-impact method that is better suited to evaluating the formation of protective films associated with the adsorption of corrosion inhibitors.

Among the three solutions studied, the concentration of 3 gl^{-1} demonstrated the most favorable results. For this concentration, a significant increase of the polarization resistance was observed after 2 days of immersion. Even after 9 days of exposure to the acidic solution, this concentration still exhibits an increasing trend for the polarization resistance.

Table 3 further shows a relevant variation of Y_1^0. The value of Y_1^0 is directly linked to the capacitance of the electrical double layer of the metallic surface through Eqs. (3)–4.

$$Z_{CPE} = Y_0^{-1}(j\omega)^{-n} \tag{3}$$

$$C_{dl} = Y\omega^{n-1}/sen[n(\pi/2)] \tag{4}$$

The constant phase elements (CPE) can be used to take into account the roughness and non-uniformity of the gray cast iron electrode. In Eq. (3), ZCPE represents the impedance value of the CPE, while ω is the angular frequency ($\omega = 2\pi f_{max}$); f_{max} is the frequency at which the imaginary component of the impedance is maximum, and n is the phase shift.

Depending on the value of n, a constant phase element (CPE) can represent different electrochemical behaviors: a resistor if $n = 0$, an inductor if $n = -1$, and a pure capacitor if $n = 1$. In the present case, the n_1 values associated with the active gray cast iron surface are consistently around 0.7–0.8 (Table 3), indicating a significant deviation from an ideal capacitive behavior. Nevertheless, the corresponding Y_0^1 values were interpreted as an indication of the effective capacitance of the charge-transfer layer. Table 3 shows a notable decrease of this apparent capacitance in the presence of the inhibitor compared to the blank solution. This reduction, together with the observed increase of the polarization resistance and inhibition efficiency, is consistent with the adsorption of the inhibitor onto the gray cast iron surface. The decrease of the effective capacitance may reflect changes of the local dielectric properties or an increase of the effective thickness of the charge-transfer layer, in line with the formation of a protective inhibitor adsorbed film.

Besides, the presence of high molecular weight chitosan in the solution leads to an increase in the absolute value of the phase angle at high frequencies compared to the blank solution (Fig. 6). This effect is also accompanied by a shift of the minimum phase angle toward higher frequencies. Even after 9 days of immersion in the presence of high molecular weight chitosan, regardless of the concentration, the phase angle at high frequency remains stable. This is associated with a higher polarization resistance and lower values of the effective capacitance of the charge-transfer layer compared to the blank sample. This behavior suggests that the main corrosion inhibition relies on the direct adsorption of chitosan on the surface of the gray cast iron, as previously indicated by the variation of the Volta potential of the gray cast iron sample after the immersion in the solution containing the inhibitor. This protection mechanism enables maintaining the inhibition efficiency close to 90 % even after 9 days of immersion in the presence of 1.5 and 3 gl^{-1} of high molecular weight chitosan in the electrolyte solution.

3.3. FE-SEM and ATR-FTIRspectroscopy measurements

In order to evaluate the adsorption mechanism of high molecular weight chitosan, the gray cast iron samples immersed for 9 days in the HCl 0.1 M electrolyte ontaining 3 gl^{-1} of the inhibitor were selected for further investigation. The morphologies of the samples after 9 days of immersion in the 0.1 M HCl solution in the presence of 3 gl^{-1} high

molecular weight chitosan are shown in Fig. 8 and compared with the blank sample immersed in the solution without the inhibitor.

In Fig. 8A, a thick and heterogeneous layer of oxides and hydroxides is formed after immersion in the blank inhibitor-free solution. In agreement with the electrochemical impedance spectroscopy spectra discussed for the blank sample, this heterogeneous layer consists of soluble corrosion products and cannot provide corrosion protection to the metallic surface. In contrast, the samples immersed in the solution containing high molecular weight chitosan (Fig. 8B) exhibit a rather uniform layer completely covering the surface.

The presence of chitosan in the protective layer of the sample shown in Fig. 8 was assessed by means of Fourier transform spectroscopy (FT-IR) in attenuated total reflectance mode (ATR).

Fig. 9A presents a comparison of the FT-IR spectra of the gray cast iron surface after 9 days of immersion in a 0.1 M HCl solution, with and without 3 gl^{-1} of chitosan. No significant signals related to organic substances could be detected on the surface of the sample immersed in the solution without inhibitor. In contrast, the spectrum obtained after immersion in the solution containing the inhibitor displays several signals related to an organic compound on the surface of the sample. Fig. 9B presents a comparison between the spectrum obtained for the surface of the gray cast iron sample corroded in the presence of chitosan and the spectrum of the pure high molecular weight chitosan powder, purchased from Sigma-Aldrich. A direct comparison of the two spectra is challenging, as several reaction products may form on the sample surface in addition to the adsorption of chitosan, and the potential presence of complexes cannot be excluded. Nonetheless, it is reasonable to infer the presence of adsorbed chitosan on the metallic surface.

Table 4 shows the main peaks connected to the spectrum of the high molecular weight chitosan and the assignment of the corresponding groups with reference to literature data. The evident band around 3334 cm^{-1} is typically connected to the hydroxyl group associated with adsorbed water and chitosan itself. The diagnostic region clearly shows the presence of peaks, around 2865 cm^{-1}, that can be associated with C—H aliphatic groups. In the fingerprint region, the peaks at 1419, 1375 cm^{-1}, and 1160 cm^{-1} can be related to the -CH_2 groups and the C—O—C groups of the -D-glucosamine units, while the large band around 1017 cm^{-1} can be assigned to the glycosidic groups that connect the different units. The presence of the peaks at 1643 and 1559 cm^{-1} may be due to N-acetyl groups and indicate that the deacetylation of the polymer is not totally completed. Peaks at similar wave numbers can also be detected for the surface of the gray cast iron sample corroded in the 0.1 M HCl solution in the presence of high molecular weight chitosan. The peaks exhibit some shifts compared to the pure chitosan powder due to a different degree of interaction between the organic molecule and the metallic surface. Nevertheless, by comparing the relative intensity of the peaks for the chitosan adsorbed on the surface of the sample, it is possible to observe a strong reduction of the peak intensity at 1017 cm^{-1} with respect to the other peaks. This reduction may be connected with the presence of a strong adsorption between the oxygen atoms in the glycosidic groups and the surface of the sample.

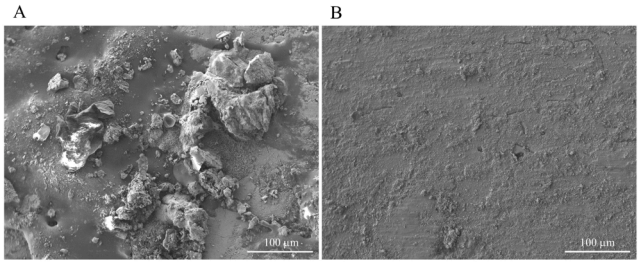

Fig. 8. FE-SEM image of the surface of the blank gray cast iron sample after 9 days of immersion in a 0.1 HCl electrolyte solution (A), FE-SEM image of the surface of the gray cast iron sample after 9 days of immersion in a 0.1 HCl solution containing 3 gl^{-1} of chitosan (B).

3.4. Conclusions

This work investigated the inhibitive properties of high molecular weight chitosan for gray cast iron that is employed for the production of brake discs in the automotive industry. The effect of high molecular weight chitosan on cast iron corrosion was evaluated by means of PDP, EIS, and SKPFM. This was complemented by characterization of the surface of gray cast iron after immersion in solutions containing the inhibitor by FE-SEM and FT-IR. From this study, it is possible to draw the following conclusions:

- High molecular weight chitosan acts as an effective corrosion inhibitor for gray cast iron in acidic environments. PDP and EIS measurements demonstrate a significant reduction of the corrosion rate for all concentrations tested in this work (0.8–1.5–3 gl^{-1}).
- Chitosan exhibits a slight influence on the cathodic reaction at early immersion times, whereas no significant effect on the anodic reaction was detected. After 1 h of immersion, PDP and SKPFM analyses reveal preferential adsorption of the inhibitor on cathodic sites (graphite flakes).
- Tafel extrapolation and polarization resistance measurements through EIS show improvements of the inhibition efficiency with chitosan concentration and immersion time. Besides, EIS fitting indicates that the increase of the total polarization resistance mainly originates from enhanced charge-transfer resistance rather than film resistance.
- Chitosan adsorption stabilizes the electrochemical behavior of gray cast iron during prolonged immersion for 9 days. In contrast with the blank sample, which shows progressive deterioration, high molecular weight chitosan-containing solutions maintain higher Rp values and stable high-frequency phase angles over time.
- FE-SEM analysis of the blank specimen and the sample immersed for 9 days in the presence of 3 gl^{-1} chitosan reveals that the inhibitor promotes the formation of a more uniform and continuous surface film, in contrast to the thick and highly heterogeneous oxide layer observed on the uninhibited sample.
- FT-IR confirms the presence of chitosan on the corroded surface after immersion. Characteristic vibrational bands of chitosan appear on the treated surface, demonstrating its incorporation into the corrosion layer.

Finally, our work indicates that high molecular weight chitosan shows promising perspectives as an organic corrosion inhibitor specifically intended for EVs. In this regard, a future study regarding the incorporation of chitosan in friction materials and its effects on the stiction phenomenon of automotive braking systems will be presented in the near future.

CRediT authorship contribution statement

Michele Motta: Writing – review & editing, Writing – original draft, Methodology, Formal analysis, Data curation, Conceptualization. **Agusti Sin:** Resources, Project administration. **Alfredo Rondinella:** Writing – review & editing, Validation, Investigation. **Lorenzo Fedrizzi:** Writing – review & editing, Supervision, Project administration, Funding acquisition. **Francesco Andreatta:** Writing – review & editing, Writing – original draft, Validation, Supervision, Project administration.

Declaration of competing interest

The authors declare that they have no known competing financial interests or personal relationships that could have appeared to influence the work reported in this paper.

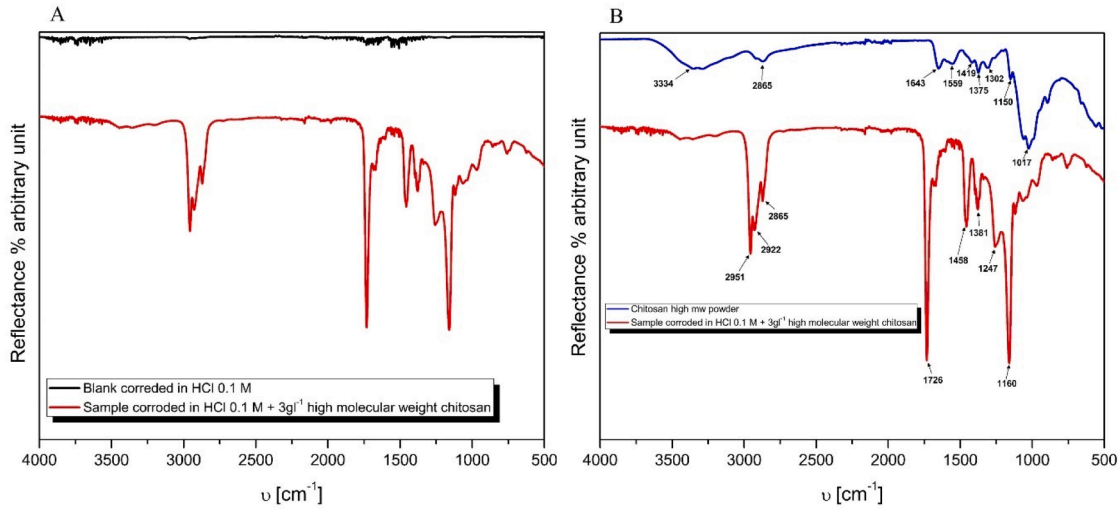

Fig. 9. FT-IR spectra of the surface of a gray cast iron sample after 9 days of immersion in a 0.1 M HCl solution and in a 0.1 M HCl solution containing 3 gl^{-1} of chitosan (A), Comparison between the FT-IR spectra of the surface of the gray cast iron sample after 9 days of immersion in a 0.1 M HCl solution containing 3 gl^{-1} of high molecular weight chitosan and pure chitosan purchased by Sigma-Aldrich (B).

Table 4
Principal characteristic vibrational bands assignment for high molecular weight chitosan (Fig. 9B).

ν [cm^{-1}]	Tentative assignment
3334	O-H [40]
2865	Aliphatic C—H [41]
1643	—CO [41]
1559	-CO in RCOO- [40]
1419	-CH_2 [41]
1375	-CH_2 [41]
1160	C-O-C group [42]
1017	CO glycosidic [43]

Data availability

Data will be made available on request.

References

[1] J. Gweon, S. Shin, H. Jang, W. Lee, D. Kim, K. Lee, The factors governing corrosion stiction of brake friction materials to a gray cast iron disc, - October, SAE Int. 2018 (2018), https://doi.org/10.4271/2018-01-1899.

[2] M. Motta, M. Zanocco, A. Rondinella, V. Iodice, A. Sin, L. Fedrizzi, et al., Inhibitive effect of 8-hydroxyquinoline on corrosion of gray cast iron in automotive braking systems, Electrochim. Acta 449 (2023), https://doi.org/10.1016/j.electacta.2023.142221.

[3] E. Apeagyei, M.S. Bank, J.D Spengler, Distribution of heavy metals in road dust along an urban-rural gradient in Massachusetts, Atmos. Env. 45 (2011) 2310–2323, https://doi.org/10.1016/j.atmosenv.2010.11.015.

[4] M. Motta, L. Fedrizzi, F. Andreatta, Corrosion stiction in automotive braking systems, Materials 16 (2023), https://doi.org/10.3390/ma16103710.

[5] V.P. Sergienko, V.V. Kozhushko, S.N. Bukharov, V.K. Merinov, Effect of corrosion inhibitors in compositions of friction composites on corrosion resistance of the metal counterbody and noise generation during friction, J. Frict. Wear 44 (2023) 259–265, https://doi.org/10.3103/S1068366623050082.

[6] J. Gweon, J. Park, W.K. Lee, D.Y. Kim, H. Jang, Root cause study of corrosion stiction by brake pads on the grey iron disc, Eng. Fail. Anal. 128 (2021), https://doi.org/10.1016/j.engfailanal.2021.105583.

[7] European Parliament, Euro 7: deal on new EU rules to reduce road transport emissions. https://WwwEuroparlEuropaEu/News/It/Press-Room/20231207IPR15740/Euro-7-Deal-on-New-Eu-Rules-to-Reduce-Road-Transport-Emissions, 2024.

[8] M. Motta, V. Iodice, A.S. Xicola, A. Truccolo, L. Fedrizzi, F. Andreatta, Role of copper and zinc additives in the stiction phenomenon of automotive braking systems, Mater. Corros. 75 (2024) 1005–1017, https://doi.org/10.1002/maco.202414322.

[9] R. Tigane, D. Bauwens, O. Hude, S. Joiret, M. Keddam, M. Turmine, et al., On the local corrosion in a thin layer of electrolyte separating two materials: specific aspects and their contribution to pad-to-disk stiction in automobile brake system, J. Solid State Electrochem. 25 (2021) 895–904, https://doi.org/10.1007/s10008-020-04867-w/Published.

[10] H. Jang, K. Ko, S.J. Kim, R.H. Basch, J.W. Fash, The effect of metal fibers on the friction performance of automotive brake friction materials, Wear 256 (2004) 406–414, https://doi.org/10.1016/S0043-1648(03)00445-9.

[11] C. Verma, M.A Quraishi, Chelation capability of chitosan and chitosan derivatives: recent developments in sustainable corrosion inhibition and metal decontamination applications, Curr. Res. Green Sustain. Chem. 4 (2021), https://doi.org/10.1016/j.crgsc.2021.100184.

[12] N.K. Gupta, P.G. Joshi, V. Srivastava, M.A. Quraishi, Chitosan: a macromolecule as green corrosion inhibitor for mild steel in sulfamic acid useful for sugar industry, Int. J. Biol. Macromol. 106 (2018) 704–711, https://doi.org/10.1016/j.ijbiomac.2017.08.064.

[13] D. Gheorghiță, H. Moldovan, A. Robu, A.I. Bița, E. Grosu, A. Antoniac, et al., Chitosan-based biomaterials for hemostatic applications: a review of recent advances, Int. J. Mol. Sci. 24 (2023), https://doi.org/10.3390/ijms241310540.

[14] D-Y Zhou, Z.-X. Wu, F.-W. Yin, S. Song, A. Li, B.-W. Zhu, et al., Chitosan and derivatives: bioactivities and application in foods, Annu. Rev. Food Sci. Technol. 12 (2021) 407–432, https://doi.org/10.1146/annurev-food-070720.

[15] S.A. Umoren, M.J. Banera, T. Alonso-Garcia, C.A. Gervasi, M.V. Mirífico, Inhibition of mild steel corrosion in HCl solution using chitosan, Cellulose 20 (2013) 2529–2545, https://doi.org/10.1007/s10570-013-0021-5.

[16] K. Vimal Kumar, B.V Appa Rao, Chemically modified biopolymer as an eco-friendly corrosion inhibitor for mild steel in a neutral chloride environment, New J. Chem. 41 (2017).

[17] G. Cui, J. Guo, Y. Zhang, Q. Zhao, S. Fu, T. Han, et al., Chitosan oligosaccharide derivatives as green corrosion inhibitors for P110 steel in a carbon-dioxide-saturated chloride solution, Carbohydr. Polym. 203 (2019) 386–395, https://doi.org/10.1016/j.carbpol.2018.09.038.

[18] H. Ashassi-Sorkhabi, A. Kazempour, Chitosan, its derivatives and composites with superior potentials for the corrosion protection of steel alloys: a comprehensive review, Carbohydr. Polym. 237 (2020), https://doi.org/10.1016/j.carbpol.2020.116110.

[19] Y. Xiaogang, S. Liyan, Z. Shufang, J. Wei, L. Yantao, H. Baorong, Corrosion inhibition properties of water soluble Chitosan and its degradation products for mild steel in seawater, J. Chin. Soc. Corros. Prot. 28 (2008).

[20] M. Naveed, L. Phil, M. Sohail, M. Hasnat, M.M.F.A. Baig, A.U. Ihsan, et al., Chitosan oligosaccharide (COS): an overview, Int. J. Biol. Macromol. 129 (2019) 827–843, https://doi.org/10.1016/j.ijbiomac.2019.01.192.

[21] D.S. Chauhan, V. Srivastava, P.G. Joshi, M.A. Quraishi, PEG cross-linked Chitosan: a biomacromolecule as corrosion inhibitor for sugar industry, Int. J. Ind. Chem. 9 (2018) 363–377, https://doi.org/10.1007/s40090-018-0165-0.

[22] V. Srivastava, D.S. Chauhan, P.G. Joshi, V. Maruthapandian, A.A. Sorour, M. A. Quraishi, PEG-functionalized Chitosan: a biological macromolecule as a novel corrosion inhibitor, ChemistrySelect 3 (2018) 1990–1998, https://doi.org/10.1002/slct.201701949.

[23] L. Guo, S. Zhu, S. Zhang, Q. He, W. Li, Theoretical studies of three triazole derivatives as corrosion inhibitors for mild steel in acidic medium, Corros. Sci. 87 (2014) 366–375, https://doi.org/10.1016/j.corsci.2014.06.040.

[24] Q. Ma, S. Qi, X. He, Y. Tang, G. Lu, 1,2,3-Triazole derivatives as corrosion inhibitors for mild steel in acidic medium: experimental and computational chemistry studies, Corros. Sci. 129 (2017) 91–101, https://doi.org/10.1016/j.corsci.2017.09.025.

[25] F. Bentiss, M. Lagrenee, M. Traisnel, J.C. Hornez, The corrosion inhibition of mild steel in acidic media by a new triazole derivative, Corros. Sci. 41 (1999) 789–803.

[26] D.S. Chauhan, M.A. Quraishi, A.A. Sorour, S.K. Saha, P. Banerjee, Triazole-modified chitosan: a biomacromolecule as a new environmentally benign corrosion inhibitor for carbon steel in a hydrochloric acid solution, RSC Adv. 9 (2019) 14990–15003, https://doi.org/10.1039/c9ra00986h.
[27] M. Rbaa, F. Benhiba, I.B. Obot, H. Oudda, I. Warad, B. Lakhrissi, et al., Two new 8-hydroxyquinoline derivatives as an efficient corrosion inhibitors for mild steel in hydrochloric acid: synthesis, electrochemical, surface morphological, UV–visible and theoretical studies, J. Mol. Liq. 276 (2019) 120–133, https://doi.org/10.1016/j.molliq.2018.11.104.
[28] W. Zhang, Y. Zhang, B. Li, H. Guo, X. Dou, K. Lu, et al., High-performance corrosion resistance of chemically-reinforced chitosan as ecofriendly inhibitor for mild steel, Bioelectrochemistry 150 (2023), https://doi.org/10.1016/j.bioelechem.2022.108330.
[29] U. Eduok, E. Ohaeri, J. Szpunar, I. Akpan, Synthesis, characterization and application of glucosyloxyethyl acrylate graft chitosan against pipeline steel corrosion, J. Mol. Liq. 315 (2020), https://doi.org/10.1016/j.molliq.2020.113772.
[30] K.E.L Mouaden, D.S. Chauhan, M.A. Quraishi, L. Bazzi, Thiocarbohydrazide-crosslinked chitosan as a bioinspired corrosion inhibitor for protection of stainless steel in 3.5% NaCl, Sustain. Chem. Pharm. 15 (2020), https://doi.org/10.1016/j.scp.2020.100213.
[31] A. Gamage, F. Shahidi, Use of chitosan for the removal of metal ion contaminants and proteins from water, Food Chem. 104 (2007) 989–996, https://doi.org/10.1016/j.foodchem.2007.01.004.
[32] D.S. Kharitonov, A.A. Kasach, A. Gibala, M. Zimowska, I.I. Kurilo, A. Wrzesinska, et al., Anodic electrodeposition of chitosan–agnp composites using in situ coordination with copper ions, Mater. (Basel) 14 (2021), https://doi.org/10.3390/ma14112754.
[33] M.M. Solomon, H. Gerengi, T. Kaya, S.A. Umoren, Performance evaluation of a chitosan/silver nanoparticles composite on St37 steel corrosion in a 15% HCl solution, ACS Sustain. Chem. Eng. 5 (2017) 809–820, https://doi.org/10.1021/acssuschemeng.6b02141.
[34] X. Lai, J. Hu, T. Ruan, J. Zhou, J. Qu, Chitosan derivative corrosion inhibitor for aluminum alloy in sodium chloride solution: a green organic/inorganic hybrid, Carbohydr. Polym. 265 (2021), https://doi.org/10.1016/j.carbpol.2021.118074.
[35] M. Li, J. Xu, R. Li, D. Wang, T. Li, M. Yuan, et al., Simple preparation of aminothiourea-modified chitosan as corrosion inhibitor and heavy metal ion adsorbent, J. Colloid Interface Sci. 417 (2014) 131–136, https://doi.org/10.1016/j.jcis.2013.11.053.
[36] M.M. Solomon, H. Gerengi, T. Kaya, E. Kaya, S.A. Umoren, Synergistic inhibition of St37 steel corrosion in 15% H2SO4 solution by chitosan and iodide ion additives, Cellulose 24 (2017) 931–950, https://doi.org/10.1007/s10570-016-1128-2.
[37] A.E. Okoronkwo, S.J. Olusegun, O.O Oluwasina, The inhibitive action of chitosan extracted from archachatina marginata shells on the corrosion of plain carbon steel in acid media, Anti-Corros. Methods Mater. 62 (2015) 13–18, https://doi.org/10.1108/ACMM-10-2013-1307.
[38] T. Rabizadeh, S. Khameneh Asl, Chitosan as a green inhibitor for mild steel corrosion: thermodynamic and electrochemical evaluations, Mater. Corros. 70 (2019) 738–748, https://doi.org/10.1002/maco.201810501.
[39] S.A. Umoren, A.A. AlAhmary, Z.M. Gasem, M.M. Solomon, Evaluation of chitosan and carboxymethyl cellulose as ecofriendly corrosion inhibitors for steel, Int. J. Biol. Macromol. 117 (2018) 1017–1028, https://doi.org/10.1016/j.ijbiomac.2018.06.014.
[40] Kuptsov A.H., Zhizhin; G.N. Handbook of Fourier transform raman and infrared spectra of polymers. 1998.
[41] A. Drabczyk, S. Kudłacik-Kramarczyk, M. Głab, M. Kedzierska, A. Jaromin, D. Mierzwiński, et al., Physicochemical investigations of chitosan-based hydrogels containing Aloe vera designed for biomedical use, Materials 13 (2020), https://doi.org/10.3390/ma13143073.
[42] S. Sahoo, C.K. Chakraborti, P.K. Behera, S.C. Mishra, FTIR and raman spectroscopic investigations of a norfloxacin/carbopol934 polymeric suspension, J. Young Pharm. 4 (2012) 138–145, https://doi.org/10.4103/0975-1483.100017.
[43] T. Hong, J.Y. Yin, S.P. Nie, M.Y Xie, Applications of infrared spectroscopy in polysaccharide structural analysis: progress, challenge and perspective, Food Chem. X 12 (2021), https://doi.org/10.1016/j.fochx.2021.100168.